Cell-substrate mechanics guide collective cell migration through intercellular adhesion: A dynamic finite element cellular model

Jieling Zhao, Farid Manuchehrfar, Jie Liang

▶ **To cite this version:**

Jieling Zhao, Farid Manuchehrfar, Jie Liang. Cell-substrate mechanics guide collective cell migration through intercellular adhesion: A dynamic finite element cellular model. Biomechanics and Modeling in Mechanobiology, 2020, 10.1007/s10237-020-01308-5 . hal-02507470

HAL Id: hal-02507470

https://hal.sorbonne-universite.fr/hal-02507470v1

Submitted on 13 Mar 2020

HAL is a multi-disciplinary open access archive for the deposit and dissemination of scientific research documents, whether they are published or not. The documents may come from teaching and research institutions in France or abroad, or from public or private research centers.

L'archive ouverte pluridisciplinaire **HAL**, est destinée au dépôt et à la diffusion de documents scientifiques de niveau recherche, publiés ou non, émanant des établissements d'enseignement et de recherche français ou étrangers, des laboratoires publics ou privés.

Noname manuscript No.
(will be inserted by the editor)

Cell-substrate mechanics guide collective cell migration through intercellular adhesion: A dynamic finite element cellular model

Jieling Zhao* · **Farid Manuchehrfar** · **Jie Liang**

Received: date / Accepted: date

Abstract During the process of tissue formation and regeneration, cells migrate collectively while remaining connected through intercellular adhesions. However, the roles of cell-substrate and cell-cell mechanical interactions in regulating collective cell migration are still unclear. In this study, we employ a newly developed finite element cellular model to study collective cell migration by exploring the effects of mechanical feedback between cell and substrate and mechanical signal transmission between adjacent cells. Our viscoelastic model of cells consists many triangular elements and is of high-resolution. Cadherin adhesion between cells are modeled explicitly as linear springs at subcellular level. In addition, we incorporate a mechanochemical feedback loop between cell-substrate mechanics and Rac-mediated cell protrusion. Our model can reproduce a number of experimentally observed patterns of collective cell migration during wound healing, including cell migration persistence, separation distance between cell pairs and migration direction. Moreover, we demonstrate that cell protrusion determined by the cell-substrate mechanics plays important role in guiding persistent and oriented collective cell migration. Furthermore, this guidance cue can be maintained and transmitted to submarginal cells of long distance through intercellular adhesions. Our study illustrates that our finite element cellular model can be employed to study broad problems of complex tissue in dynamic changes at subcellular level.

Keywords Collective cell migration · Finite element model · Cell-substrate mechanics · Intercellular adhesion · DyCelFEM

*: corresponding author
Jieling Zhao* (ORCID: 0000-0002-9801-2434)
INRIA de Paris and Sorbonne Universités UPMC, LJLL Team Mamba
Paris, France
E-mail: jieling.zhao@inria.fr

Farid Manuchehrfar · Jie Liang (ORCID: 0000-0002-2773-6427)
Department of Bioengineering
University of Illinois at Chicago
Chicago, USA

1 Introduction

Cells are the fundamental units of living body. They undergo programmed motilities and rearrangements to form biological tissues (Alberts, 2008). During the process of tissue formation and regeneration such as embryonic development, organ morphogenesis, and wound healing, cells migrate collectively as adherent groups (Friedl and Gilmour, 2009; Rørth, 2007). Unlike the mechanism of single cell migration, which has been extensively investigated and well understood at subcellular level (Lauffenburger and Horwitz, 1996; Lautscham et al., 2015; Ridley et al., 2003), the mechanisms behind collective cell migration are still unclear.

A great number of experimental studies have characterized how cells respond to changes in the extracellular matrix (ECM) or substrate (Leong et al., 2013; Sheets et al., 2013; Watt and Huck, 2013). These studies indicated that changes in the topography or stiffness of the ECM provide physical and geometric cues to initiate or regulate different cell behaviors (Nikkhah et al., 2012; Rape et al., 2011). Specifically for the behavior of cell migration, cells deform their bodies and polarize in response to these cues and then initiate the actinmyosin-related pathways to migrate (Wolf et al., 2013). While cells migrate in groups, they also generate intercellular mechanical forces spontaneously to form

an integrity unit (Tambe et al., 2011). Changes in these mechanical forces from the leading cell in the group can be sensed by its neighboring cells via intercellular adhesions (Weber et al., 2012). Proteins such as cadherin complex and α-catenin have been reported to play important roles in facilitating transmission of mechanical forces between neighboring cells (Benjamin et al., 2010; Ng et al., 2012).

However, it remains difficulty to experimentally access the underlying mechanical forces during collective cell migration such as forces generated from cytoskeleton due to cell anchoring on ECM (Brugués et al., 2014) and forces exerted at cell-cell junctions (Tambe et al., 2011; Trepat et al., 2009), many questions regarding how collective cell migration is regulated by mechanical forces through cell-ECM contact and intercellular adhesions are still open. For example, how does the force generated from the moving cell propel the collective cell movement (Kim et al., 2013)? How does the propagation of mechanical signals contribute to mechanical connection between moving cells (Defranco et al., 2008)?

Recently, computational models have become increasingly useful to complement experimental observations towards understanding the mechanisms of collective cell migration. A number of computational cell models have been developed to study the mechanical interactions between cells or between cell and ECM (Albert and Schwarz, 2016; Basan et al., 2013; Checa et al., 2015; Drasdo and Hoehme, 2012; Hoehme and Drasdo, 2010; Hutson et al., 2009; Kabla, 2012; Kachalo et al., 2015; Kim et al., 2018, 2015; Lee and Wolgemuth, 2011; Lee et al., 2017; Marée et al., 2007; Merchant et al., 2018; Nagai and Honda, 2009; Nematbakhsh et al., 2017; Sandersius et al., 2011; Van Liedekerke et al., 2019; Vermolen and Gefen, 2015; Vitorino et al., 2011; Zhao et al., 2013). However, these models have limitations. Some discrete models regard cells as simple objects of spheres or squares, without account for details of cell morphology (Basan et al., 2013; Checa et al., 2015; Drasdo and Hoehme, 2012; Hoehme and Drasdo, 2010; Lee et al., 2017). In continuum models, cells are considered implicitly as viscoelastic flows, the effects of cellular boundary forces are not well treated (Lee and Wolgemuth, 2011). In cellular Potts model, changes in cellular shapes are often represented as state changes of lattice sites. However the underlying physical forces and cellular mechanics are difficult to recover (Albert and Schwarz, 2016; Marée et al., 2007). Vertex models describe the changes in cell shape based on minimizing energy under forces exerting on cell boundary. However, the contribution of specific cell shape to the mechanical energy of cell interior is not well considered (Kabla, 2012; Kachalo et al., 2015; Vitorino et al., 2011). Finite element models have also been developed, but they only allowed limited changes in cell shape and limited flexibility in cell movement (Hutson et al., 2009; Vermolen and Gefen, 2015; Zhao et al., 2013). Other models mimic the cellular mechanics using arbitrarily imposed Morse potential which is unrealistic at cellular level (Nematbakhsh et al., 2017; Sandersius et al., 2011). In many cases, details of the intercellular adhesions are not considered (Basan et al., 2013; Checa et al., 2015; Drasdo and Hoehme, 2012; Hoehme and Drasdo, 2010; Hutson et al., 2009; Kabla, 2012; Kim et al., 2018, 2015; Lee and Wolgemuth, 2011; Lee et al., 2017; Merchant et al., 2018; Nagai and Honda, 2009; Van Liedekerke et al., 2019; Vermolen and Gefen, 2015; Vitorino et al., 2011).

In this study, we presented a novel theoretical model to explore the role of cell-substrate contact and intercellular adhesions on collective cell migration. Our model describes each cell by a mesh of discrete sub-cellular triangular elements. Each element is assigned with viscoelastic property using a Maxwellian model (Karcher et al., 2003). The effects of curvature-dependent line tension forces along the cell boundary is also incorporated (Oakes et al., 2014). The intercellular adhesion is modeled explicitly as elastic springs at real scale (Jamali et al., 2010). In addition, a mechano-chemical pathway involving mechanical-induced focal adhesion and proteins Paxillin, Rac, PAK, and Merlin, which are responsible for cell protrusion (Cirit et al., 2010) is embedded in each cell. This pathway is supplemented by another mechano-chemical pathway, which is responsible for the transmission of mechanical cue through intercellular adhesion (Okada et al., 2005). Our model is applied to simulate collective cell migration using a simplified wound tissue. Our simulation results are then compared to an *in vitro* study (Ng et al., 2012). Finally, we discussed our results and drew the conclusion that the cell-substrate mechanics play important role in guiding collective cell migration with high efficiency. This guidance cue is maintained and transmitted to cells within the group of cells by intercellular adhesions.

2 Mathematical model of mechanics of cells

2.1 Geometric model of cells

In our model, a two-dimensional cell $\Omega \subset \mathbb{R}^2$ is represented as an oriented polygon connecting a set of boundary vertices $V_{\partial\Omega} \equiv \{\boldsymbol{v}_i \in \partial\Omega \subset \mathbb{R}^2\}$, with the location of the vertex $\boldsymbol{v}_i$ denoted as $\boldsymbol{x}_i$. The set of boundary vertices $V_{\partial\Omega}$, along with a set of internal vertices V_{Int} and a set of triangular elements $T_\Omega \equiv$

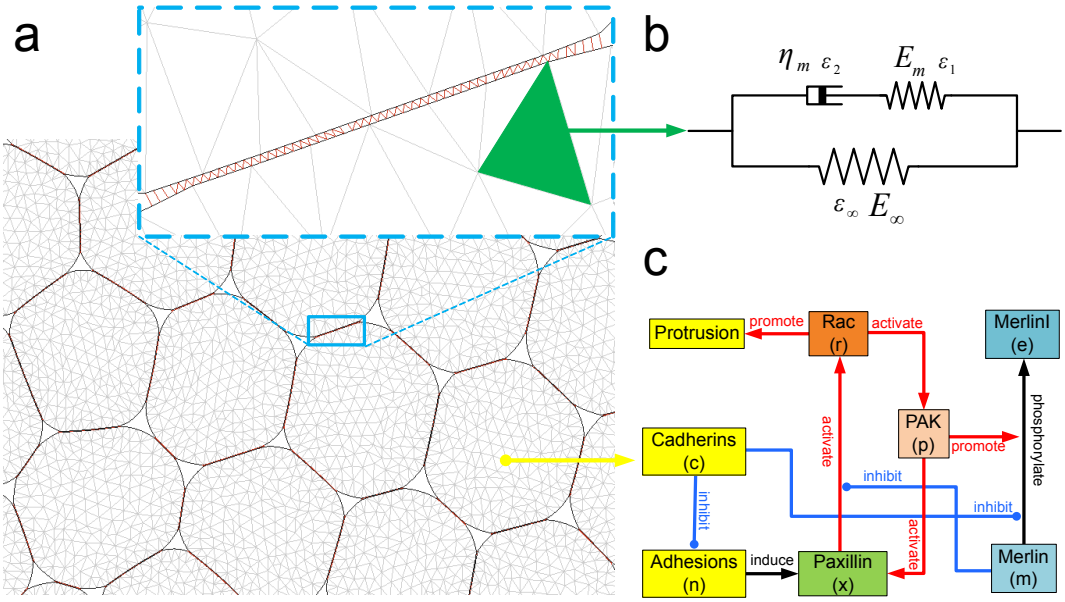

Fig. 1 Geometric model of the cell and the chemical signaling pathway regulating cell-substrate contact and intercellular adhesion. (a) The cell represented in our model: the boundary of each cell is defined by an oriented polygon containing a number of boundary vertices. Triangular mesh tiling up each cell is then constructed based on farthest sampling method (Zhao et al., 2017). The E-cadhesion type of the intercellular junctions between two adherent cells are modeled as elastic springs (red bars in the blue box, a closer view in the enlarged dashed blue box). (b) Viscoelastic property is assigned to each triangular element using a generalized Maxwell model following previous studies (Karcher et al., 2003; Schoner et al., 2004; Schwartz et al., 2005). (c) The positive feedback network between focal adhesion and cell protrusion is embedded onto each vertex of the triangular mesh following (Cirit et al., 2010). This signaling network involves proteins integrin, Paxillin, Rac, and PAK. The cadherin-containing protein Merlin is also incorporated into this network to count the effects of intercellular adhesion on cell migration (Okada et al., 2005).

$\{\boldsymbol{\tau}_{i,j,k} : \boldsymbol{v}_i, \boldsymbol{v}_j, \boldsymbol{v}_k \in V_{\partial\Omega} \cup V_{\text{Int}}\}$ define the geometry of Ω (Fig. 1a, see more details of generating V_{Int} and T_Ω in (Zhao et al., 2017)). If two cells are in contact with each other, they are connected by adhesive springs between them (Fig. 1a, red bars in the dashed blue box). Each cell boundary edge has several interior vertice evenly distributed along the edge. These interior vertice are the potential locations for the adhesive spring to be attached. Any force exerted on that interior vertex through the adhesive spring will be projected onto its nearest end-node vertex of the corresponding boundary edge (see more details of modeling the adhesive springs and the sensitivity test of number of interior vertice in Supplementary Information).

2.2 Viscoelastic cell model

Previous studies have demonstrated that the cell cytoskeleton network exhibits viscoelastic properties (Ladoux et al., 2016; Rubinstein et al., 2009). Following studies of (Barnhart et al., 2011; Dokukina and Gracheva, 2010), we assume that linear viscoelasticity can adequately describe the mechanical properties of the cell during cell deformation and cell migration.

2.2.1 Strain and stress tensors

We use the strain tensor $\boldsymbol{\epsilon}(\boldsymbol{x},t)$ to describe the local deformation of the cell at $\boldsymbol{x}$ at time t. $\boldsymbol{\epsilon}(\boldsymbol{x},t)$ takes the form of $\epsilon_{1,1} = \partial u_1/\partial x_1$, $\epsilon_{2,2} = \partial u_2/\partial x_2$, and $\epsilon_{1,2} = \epsilon_{2,1} = \frac{1}{2}(\partial u_1/\partial x_2 + \partial u_2/\partial x_1)$, where $\boldsymbol{u}(\boldsymbol{x},t)$ defined as $(u_1(\boldsymbol{x},t), u_2(\boldsymbol{x},t))^T \subset \mathbb{R}^2$ is the displacement of $\boldsymbol{x}$ at time t.

We use the stress tensor $\boldsymbol{\sigma}(\boldsymbol{x},t)$ to represent the forces at $\boldsymbol{x}$ at time t. Here $\boldsymbol{\sigma}$ is related to the strain tensor $\boldsymbol{\epsilon}$ through a generalized Maxwell model: $\boldsymbol{\sigma}(\boldsymbol{x},t) = \boldsymbol{\sigma}_\infty(\boldsymbol{x},t) + \boldsymbol{\sigma}_m(\boldsymbol{x},t)$ (Karcher et al., 2003; Schoner et al., 2004; Schwartz et al., 2005), where $\boldsymbol{\sigma}_\infty(\boldsymbol{x},t)$ is the stress of the long-term elastic element and $\boldsymbol{\sigma}_m(\boldsymbol{x},t)$ is the stress of the Maxwell elastic element. The long-term elastic modulus, elastic modulus of the Maxwell elastic element, and viscous coefficient of the Maxwell viscous element are denoted as E_∞, E_m, and η_m, respectively (Fig. 1b). From the mechanical property of the generalized Maxwell model, the strain of the Maxwell elastic element $\boldsymbol{\epsilon}_1(\boldsymbol{x},t)$ and the strain of the viscous element $\boldsymbol{\epsilon}_2(\boldsymbol{x},t)$ add up to the strain tensor $\boldsymbol{\epsilon}(\boldsymbol{x},t)$: $\boldsymbol{\epsilon}_1(\boldsymbol{x},t) + \boldsymbol{\epsilon}_2(\boldsymbol{x},t) = \boldsymbol{\epsilon}(\boldsymbol{x},t)$.

We assume that the total free energy of one cell is the sum of cell's elastic energy, adhesion energy due to

contact with the substrate, elastic energy due to intercellular adhesions with other cells, and the energy due to cell boundary forces.

2.2.2 Elastic energy of the cell

The elastic energy associated with the deformation contributes to the total energy $E_\Omega(t)$ of the cell Ω. It is given by

$$E_\Omega(t) = \frac{1}{2}\int_\Omega (\boldsymbol{\sigma}_\infty(\boldsymbol{x},t) + \sigma_a \boldsymbol{\delta}_{ij}(\boldsymbol{x}))^T \boldsymbol{\epsilon}(\boldsymbol{x},t) d\boldsymbol{x} + \frac{1}{2}\int_\Omega \boldsymbol{\sigma}_m(\boldsymbol{x},t)^T \boldsymbol{\epsilon}_1(\boldsymbol{x},t) d\boldsymbol{x}, \quad (1)$$

where σ_a is a homogeneous contractile pressure (Oakes et al., 2014).

2.2.3 Adhesion energy due to cell-substrate contact

The energy due to the adhesion between cell and substrate also contributes to the total energy of the cell, which is given by (Oakes et al., 2014)

$$\frac{Y(\boldsymbol{x},t)}{2}\int_\Omega \boldsymbol{u}(\boldsymbol{x},t)^2 d\boldsymbol{x}, \quad (2)$$

where $Y(\boldsymbol{x},t)$ is the adhesion coefficient at time t and set to be proportional to the strength of focal adhesions (Banerjee and Marchetti, 2012): $Y(\boldsymbol{x},t) = \frac{n_{\boldsymbol{x},t}}{n_0} E_{st} Y_a$, where $n_{\boldsymbol{x},t}$ is the number of bound integrins at location $\boldsymbol{x}$ at t (see details of calculation of $n_{\boldsymbol{x},t}$ in the section of **Model of focal adhesion**), n_0 is a normalizing constant number, E_{st} is the stiffness of the substrate and Y_a is the basic adhesion constant taken from (Banerjee and Marchetti, 2012).

2.2.4 Adhesion energy due to intercellular adhesion

The intercellular adhesions, modeled as elastic springs, also contribute to the total energy of the cell. This is given by $\frac{1}{2}\sum_l k_l \boldsymbol{u}_l(t)^2$, where k_l is the spring constant of the adhesion spring l. Denoting the spring's orientation angle as $\theta_l(t)$ at time t and the transformation vector $T(\theta)$ as $(\cos(\theta_l), \sin(\theta_l), -\cos(\theta_l), -\sin(\theta_l))$, $\boldsymbol{u}_l(t)$ can be written as $\boldsymbol{u}_l(t) = T(\theta_l)(\boldsymbol{u}_{11}(t), \boldsymbol{u}_{l2}(t))$, where $\boldsymbol{u}_{l1}(t)$ and $\boldsymbol{u}_{l2}(t)$ are the displacements of l's two end-node vertice $\boldsymbol{x}_1$ and $\boldsymbol{x}_2$ at time t. The elastic force of l due to displacement of Δl is applied on $\boldsymbol{x}_i$ and $\boldsymbol{x}_j$ as $\boldsymbol{f}_l = f(\Delta l)\boldsymbol{e}_l$ and -$f(\Delta l)\boldsymbol{e}_l$, respectively, where $f(\Delta l)$ is the magnitude of the elastic force, $\boldsymbol{e}_l$ is the unit vector of the orientation of l.

2.2.5 Boundary and protrusion forces

Furthermore, the local forces applied on the cell boundary also contribute to the energy. Following (Oakes et al., 2014), we consider the tension force generated by actomyosin fibers along the cell boundary. In addition, we also incorporate the protrusion force generated by actin polymerization on the leading edge of migrating cell. These contributions can be written as

$$\int_{\partial\Omega} (\boldsymbol{\lambda}(\boldsymbol{x},t) + \boldsymbol{f}(\boldsymbol{x},t))\boldsymbol{u}(\boldsymbol{x},t) d\boldsymbol{x}, \quad (3)$$

where $\boldsymbol{\lambda}(\boldsymbol{x},t)$ is the line tension force and $\boldsymbol{f}(\boldsymbol{x},t)$ is the protrusion force. Line tension force is written as $\boldsymbol{\lambda}(\boldsymbol{x},t) = -f_m \kappa(\boldsymbol{x},t)\boldsymbol{n}(\boldsymbol{x},t)$, where f_m is a contractile force per unit length, $\kappa(\boldsymbol{x},t)$ is the curvature, and $\boldsymbol{n}(\boldsymbol{x},t)$ is the outward unit normal at $\boldsymbol{x}$ at time t (Oakes et al., 2014). Protrusion force is represented as $\boldsymbol{f}(\boldsymbol{x},t) = -f_a \boldsymbol{n}(\boldsymbol{x},t)$, where f_a is the protrusion force per unit length (see more details of cell protrusion model in supplementary Information).

2.2.6 The total free energy and its dissipation

In summary, the total free energy for cell Ω at time t is given by

$$\begin{aligned} E_\Omega(t) = {} & \frac{1}{2}\int_\Omega ((\boldsymbol{\sigma}_\infty(\boldsymbol{x},t) + \boldsymbol{\sigma}_a \delta_{ij})^T \boldsymbol{\epsilon}(\boldsymbol{x},t) \\ & + \boldsymbol{\sigma}_m^T(\boldsymbol{x},t)\boldsymbol{\epsilon}_1(\boldsymbol{x},t))d\boldsymbol{x} + \frac{1}{2}\int_\Omega (\sigma_a, \sigma_a, 0)\boldsymbol{\epsilon}(\boldsymbol{x},t) d\boldsymbol{x} \\ & + \frac{Y(\boldsymbol{x},t)}{2}\int_\Omega \boldsymbol{u}(\boldsymbol{x},t)^2 d\boldsymbol{x} + \frac{1}{2}\sum_l k_l \boldsymbol{u}_l(t)^2 \\ & + \int_{\partial\Omega} (\boldsymbol{\lambda}(\boldsymbol{x},t) + \boldsymbol{f}(\boldsymbol{x},t) + \boldsymbol{f}_l(\boldsymbol{x},t))\boldsymbol{u}(\boldsymbol{x},t) d\boldsymbol{x}). \end{aligned} \quad (4)$$

The energy dissipation of the total free energy due to cell viscosity is determined by the viscous coefficient η_m and the strain of the viscous element $\boldsymbol{\epsilon}_2(\boldsymbol{x},t)$ (Sedef et al., 2006): $-\int_\Omega \eta_m (\frac{\partial \boldsymbol{\epsilon}_2}{\partial t})^2 d\boldsymbol{x}$. The dissipation of the total free energy of the cell can then be written as

$$\begin{aligned} \frac{\partial}{\partial t} E_\Omega(t) = {} & \frac{\partial}{\partial t}(\frac{1}{2}\int_\Omega ((\boldsymbol{\sigma}_\infty(\boldsymbol{x},t) + \boldsymbol{\sigma}_a \delta_{ij})^T \boldsymbol{\epsilon}(\boldsymbol{x},t) \\ & + \boldsymbol{\sigma}_m^T(\boldsymbol{x},t)\boldsymbol{\epsilon}_1(\boldsymbol{x},t))d\boldsymbol{x} + \frac{1}{2}\int_\Omega (\sigma_a, \sigma_a, 0)\boldsymbol{\epsilon}(\boldsymbol{x},t) d\boldsymbol{x} \\ & + \frac{Y(\boldsymbol{x},t)}{2}\int_\Omega \boldsymbol{u}(\boldsymbol{x},t)^2 d\boldsymbol{x} + \frac{1}{2}\sum_l k_l \boldsymbol{u}_l(t)^2 \\ & + \int_{\partial\Omega} (\boldsymbol{\lambda}(\boldsymbol{x},t) + \boldsymbol{f}(\boldsymbol{x},t) + \boldsymbol{f}_l(\boldsymbol{x},t))\boldsymbol{u}(\boldsymbol{x},t) d\boldsymbol{x}) \\ = {} & -\int_\Omega \eta_m (\frac{\partial \boldsymbol{\epsilon}_2(\boldsymbol{x},t)}{\partial t})^2 d\boldsymbol{x}. \end{aligned} \quad (5)$$

Since $\eta_m \frac{\partial \boldsymbol{\epsilon}_2}{\partial t} = E_m \boldsymbol{\epsilon}_1$ and $\boldsymbol{\sigma}_\infty = E_\infty \boldsymbol{\epsilon}$, and $\boldsymbol{u}_l(t) = T(\theta_l)(\boldsymbol{u}_{l1}, \boldsymbol{u}_{l2})$. Eqn (5) can be rewritten as

$$\begin{aligned}
&\int_\Omega E_\infty \boldsymbol{\epsilon}(\boldsymbol{x},t) \frac{\partial \boldsymbol{\epsilon}(\boldsymbol{x},t)}{\partial t} d\boldsymbol{x} + \int_\Omega \boldsymbol{\sigma}_m^T(\boldsymbol{x},t) \frac{\partial \boldsymbol{\epsilon}(\boldsymbol{x},t)}{\partial t} d\boldsymbol{x} \\
&+ \int_\Omega (\sigma_a, \sigma_a, 0) \frac{\partial \boldsymbol{\epsilon}(\boldsymbol{x},t)}{\partial t} d\boldsymbol{x} + Y \int_\Omega \boldsymbol{u}(\boldsymbol{x},t) \frac{\partial \boldsymbol{u}(\boldsymbol{x},t)}{\partial t} d\boldsymbol{x} \\
&+ \sum_l T(\theta_l)^T T(\theta_l) k_l(\boldsymbol{u}_{l1}(t), \boldsymbol{u}_{l2}(t)) \frac{\partial \boldsymbol{u}(\boldsymbol{x},t)}{\partial t} \\
&+ \int_{\partial\Omega} (\boldsymbol{\lambda}(\boldsymbol{x},t) + \boldsymbol{f}(\boldsymbol{x},t) + \boldsymbol{f}_l(\boldsymbol{x},t)) \frac{\partial \boldsymbol{u}(\boldsymbol{x},t)}{\partial t} d\boldsymbol{x} = 0.
\end{aligned} \tag{6}$$

Denoting $\boldsymbol{B} = \begin{pmatrix} \partial/\partial x_1 & 0 \\ 0 & \partial/\partial x_2 \\ \partial/\partial x_2 & \partial/\partial x_1 \end{pmatrix}$, then $\boldsymbol{\epsilon}(\boldsymbol{x},t) = \boldsymbol{B}\boldsymbol{u}(\boldsymbol{x},t)$. According to Gauss' divergence theorem, we rewrote $\int_\Omega (\sigma_a, \sigma_a, 0) \boldsymbol{B} \frac{\partial \boldsymbol{u}(\boldsymbol{x},t)}{\partial t}$ as $\int_\Omega \sigma_a \nabla \cdot \frac{\partial \boldsymbol{u}(\boldsymbol{x},t)}{\partial t} d\boldsymbol{x}$, which equals to $\int_{\partial\Omega} \sigma_a \boldsymbol{n}(\boldsymbol{x},t) \frac{\partial \boldsymbol{u}(\boldsymbol{x},t)}{\partial t} d\boldsymbol{x}$.

Denoting $\boldsymbol{A}_l = \begin{pmatrix} c_l^2 & c_l s_l & -c_l^2 & -c_l s_l \\ c_l s_l & s_l^2 & -c_l s_l & -s_l^2 \\ -c_l^2 & -c_l s_l & c_l^2 & c_l s_l \\ -c_l s_l & -s_l^2 & c_l s_l & s_l^2 \end{pmatrix}$, where $c_l = cos(\theta_l)$ and $s_l = sin(\theta_l)$. Eqn (6) can be rewritten as

$$\begin{aligned}
&\int_\Omega \boldsymbol{B}^T \boldsymbol{\sigma}(\boldsymbol{x},t)^T d\boldsymbol{x} + Y \int_\Omega \boldsymbol{u}(\boldsymbol{x},t) d\boldsymbol{x} \\
&+ \sum_l \boldsymbol{A}_l k_l(\boldsymbol{u}_{l1}(t), \boldsymbol{u}_{l2}(t)) = \\
&- \int_{\partial\Omega} \sigma_a \boldsymbol{n}(\boldsymbol{x},t) + \boldsymbol{\lambda}(\boldsymbol{x},t) + \boldsymbol{f}(\boldsymbol{x},t) + \boldsymbol{f}_l(\boldsymbol{x},t) d\boldsymbol{x}
\end{aligned} \tag{7}$$

2.2.7 Stress of viscoelastic cell and its update

From the mechanical property of the general Maxwell model, the stress $\boldsymbol{\sigma}(\boldsymbol{x},t)$ can be written as (Schoner et al., 2004; Schwartz et al., 2005; Sedef et al., 2006):

$$\begin{aligned}
&E_\infty \boldsymbol{\epsilon}(\boldsymbol{x},t) + \int_0^t E_m e^{\frac{t-s}{\eta_m / E_\infty}} \frac{\partial \boldsymbol{\epsilon}(\boldsymbol{x},s)}{\partial s} ds = \\
&\boldsymbol{\sigma}_\infty(\boldsymbol{x},t) + \boldsymbol{\sigma}_m(\boldsymbol{x},t).
\end{aligned} \tag{8}$$

During the time interval $\Delta t = t_{n+1} - t_n$, where t_n is the n-th time step, $\boldsymbol{\sigma}_m^{n+1}(\boldsymbol{x})$ can be written as (Sedef et al., 2006):

$$\begin{aligned}
&e^{-\frac{\Delta t}{\eta_m / E_\infty}} \boldsymbol{\sigma}_m^n(\boldsymbol{x}) + \\
&\frac{E_m}{E_\infty} \int_{t_n}^{t_{n+1}} e^{-\frac{t_{n+1}-s}{\eta_m / E_\infty}} ds \frac{\boldsymbol{\sigma}_\infty^{n+1}(\boldsymbol{x}) - \boldsymbol{\sigma}_\infty^n(\boldsymbol{x})}{\Delta t}.
\end{aligned} \tag{9}$$

Therefore, the stress $\boldsymbol{\sigma}^n(\boldsymbol{x})$ at t_n can be written as

$$\boldsymbol{\sigma}^n(\boldsymbol{x}) = \boldsymbol{\sigma}_\infty^n(\boldsymbol{x}) + \boldsymbol{\sigma}_m^n(\boldsymbol{x}) \tag{10}$$

2.2.8 Force balance equation for discretized time step

For each triangular element $\boldsymbol{\tau}_{i,j,k}$, Eqn (7) at time step t_{n+1} can be rewritten using Eqn (10) as

$$\begin{aligned}
&\int_{\boldsymbol{\tau}_{i,j,k}} \boldsymbol{B}^T (E_\infty \boldsymbol{B} \boldsymbol{u}^{n+1}(\boldsymbol{x}) + e^{-\frac{\Delta t}{\eta_m / E_\infty}} \boldsymbol{\sigma}_m^n \\
&+ \gamma_m A_m (E_\infty \boldsymbol{B} \boldsymbol{u}^{n+1}(\boldsymbol{x}) - E_\infty \boldsymbol{B} \boldsymbol{u}^n(\boldsymbol{x}))) d\boldsymbol{x} \\
&+ Y \int_{\boldsymbol{\tau}_{i,j,k}} \boldsymbol{u}^{n+1} d\boldsymbol{x} + \sum_{l \in \boldsymbol{\tau}_{i,j,k}} \boldsymbol{A}_l k_l(\boldsymbol{u}_{l1}^{n+1}, \boldsymbol{u}_{l2}^{n+1}) = \boldsymbol{F}^{n+1}(\boldsymbol{x}),
\end{aligned} \tag{11}$$

where $\gamma_m = E_m / E_\infty$, $A_m = \frac{1 - e^{-\frac{\Delta t}{\eta_m / E_\infty}}}{\frac{\Delta t}{\eta_m / E_\infty}}$, and $\boldsymbol{F}^{n+1} = -\int_{\partial\Omega} \sigma_a \boldsymbol{n}(\boldsymbol{x},t) + \boldsymbol{\lambda}(\boldsymbol{x},t) + \boldsymbol{f}(\boldsymbol{x},t) + \boldsymbol{f}_l(\boldsymbol{x},t) d\boldsymbol{x}$. Eqn (11) eventually leads to the corresponding linear force-balance equation

$$\boldsymbol{K}_{\boldsymbol{\tau}_{i,j,k}}^{n+1} \boldsymbol{u}_{\boldsymbol{\tau}_{i,j,k}}^{n+1} = \boldsymbol{f}_{\boldsymbol{\tau}_{i,j,k}}^{n+1}, \tag{12}$$

where $\boldsymbol{K}_{\boldsymbol{\tau}_{i,j,k}}^{n+1}$, $\boldsymbol{u}_{\boldsymbol{\tau}_{i,j,k}}^{n+1}$, and $\boldsymbol{f}_{\boldsymbol{\tau}_{i,j,k}}^{n+1}$ are the stiffness matrix, displacement vector, and integrated force vector of $\boldsymbol{\tau}_{i,j,k}$ at time step t_{n+1} (see more details of derivation of (Eqn 12) in (Zhao et al., 2017)).

We can then gather the element stiffness matrices of all triangular elements in every cell and assemble them into one global stiffness matrix $\boldsymbol{K}^{n+1}$. The linear relationship between the concatenated displacement vector $\boldsymbol{u}^{n+1}$ of all vertice in all cells and the integrated force vector $\boldsymbol{f}^{n+1}$ on all vertice is then given by

$$\boldsymbol{K}^{n+1} \boldsymbol{u}^{n+1} = \boldsymbol{f}^{n+1}. \tag{13}$$

Changes in the cell shape at time step t_{n+1} can then be obtained by solving Eqn 13. For vertex $\boldsymbol{v}_i$ at $\boldsymbol{x}_i$, its new location at next time step is then updated as $\boldsymbol{x}_i^{n+1} = \boldsymbol{x}_i^n + \boldsymbol{u}^{n+1}(\boldsymbol{v}_i)$.

2.3 Mechano-chemical pathway in the cell

Upon contact with the ECM or substrate, cells transfer the mechanical stimulus into biochemical signals, which then lead to the initiation of additional cellular behaviors (Holle and Engler, 2011). In our model, we considered a mechao-chemical pathway consisting of two parts. One is responsible for regulating the feedback loop between focal adhesion and cell protrusion. The other is responsible for the mechanical signal transmission between adjacent cells through intercellular adhesions.

2.3.1 Model of focal adhesion

For each vertex $\boldsymbol{v}_i$ in cell Ω, we assume that there is a constant number of integrin ligand. These integrin molecules bind and unbind with fibronectin molecules on the substrate underneath. Following (DiMilla et al., 1991), the numbers of bound and unbound integrin ligand molecules are governed by

$$\frac{dR_b}{dt} = k_f n_s R_u - k_r R_b, \tag{14}$$

where R_u and R_b are the numbers of unbound and bound integrin ligand, respectively; k_f is the binding rate constant, namely, the rate of free ligand becomes bound ligand; n_s is the uniform concentration of fibronectin per vertex; k_r is the unbinding rate, namely, the rate of bound ligand becomes unbound ligand. k_r depends on the traction force $\boldsymbol{f}_r$ applied on $\boldsymbol{v}_i$. Traction force $\boldsymbol{f}_r(\boldsymbol{x}, t)$ on $\boldsymbol{x}$ at time t is calculated as $Y(\boldsymbol{x}, t)\boldsymbol{u}(\boldsymbol{x}, t)$ following (Oakes et al., 2014). We followed a previous study (Li et al., 2010) to determine k_r as $k_r = k_{r_0}(e^{-0.04f_r} + 4e - 7e^{0.2f_r})$, where k_{r_0} is a constant. We related k_f with the substrate stiffness by $k_f = k_{f0}E_{st}^2/(E_{st}^2 + E_{st0}^2)$ (Dokukina and Gracheva, 2010; Yeh et al., 2017), where k_{f0} and E_{st0} are constants (see supplementary Information for choosing E_{st0}).

2.3.2 Model of feedback loop between focal adhesion and cell protrusion

We used a simplified model of a positive feedback loop to control the spatial distribution of the focal adhesions, which determines the direction of cell protrusion (Cirit et al., 2010; Stéphanou et al., 2008). In our model, this feedback loop consists of proteins Paxillin, Rac, and PAK (Fig. 1c). Upon formation of focal adhesion, Paxillin is activated through the phosphorylation of active PAK. The activated Paxillin then activates Rac, which in turn activates PAK. The activated Rac is responsible for cell protrusion (Wu et al., 2009). Since the protein Merlin on the cell-cell cadherin complex also plays a role in activating Rac (Okada et al., 2005), we incorporate Merlin in our feedback loop as well. Specifically, the concentrations of the proteins over time are updated through a set of differential equations following (Cirit et al., 2010):

$$\frac{dr}{dt} = k_{x,r}(k_m \frac{C_r^2}{C_r^2 + m^2} x - r) \tag{15}$$

$$\frac{dp}{dt} = k_{r,p}(r - p) \tag{16}$$

$$\frac{dx}{dt} = k_{p,x}(k_x \frac{p^2}{p^2 + C_x^2} n - x) \tag{17}$$

where x, r, p, m and n are the concentrations of activated Paxillin, activated Rac, activated PAK, Merlin and bound integrins, respectively. $k_{x,r}$, $k_{r,p}$, $k_{p,x}$, k_m, k_x, C_r, C_x are the corresponding rate parameters. The level of activated Rac was then used to determine the cell protrusion force on the leading edge of the migrating cell (see details of cell protrusion model in supplementary Information).

2.3.3 Model of mechanosensing through intercellular adhesion

We incorporated Merlin in the feedback loop (Fig. 1c) following a previous report that Merlin on the cell-cell cadherin complex regulates the activity of Rac (Das et al., 2015). As illustrated in Fig. 2a, for two neighboring cells C_1 and C_2 where C_1 is the leader cell and C_2 is the follower cell, if both are at static state, Merlin molecules will be located on the two ends of the cadherin spring (Fig. 2b top). As reported in (Okada et al., 2005), Merlin suppressed the binding of integrin. As a consequence, Rac is inactivated on the Merlin-expressed site. If cell C_1 starts to migrate, there will be tension force generated on the cadherin spring between C_1 and C_2. Merlin is then delocalized from the cadherin site in response to the tension force. As a consequence, Rac is activated on that site to generate protrusion to follow the leader cell (Fig. 2b bottom (Das et al., 2015)). For simplicity, we introduced an inactive Merlin along with the active Merlin on the two end vertice of one intercellular adhesion. The Merlin-Rac negative feedback loop is then modeled through a set of differential equations (Das et al., 2015; Okada et al., 2005), where active Merlin and inactive Merlin can convert from each other, where only active Merlin can suppress the Rac acitivity through the positive feedback loop (Fig. 1c).

The delocalization of Merlin was simply modeled as Merlin transforming into inactive mode:

$$\frac{dm}{dt} = e - \delta(f_t > f_{t-thr})k_{m,e}(k_p(\frac{p^2}{p^2 + C_e^2} + k_e)m \tag{18}$$

$$\frac{de}{dt} = \delta(f_t > f_{t-thr})k_{m,e}(k_p(\frac{p^2}{p^2 + C_e^2} + k_e)m) - e \tag{19}$$

where m, e and p are the concentrations of Merlin, inactive Merlin, and PAK, respectively. $k_{m,e}$, k_p, k_e, C_e are the corresponding rate parameters. $\delta(x)$ is a kronecker function that $\delta(TRUE) = 1$ and $\delta(FALSE) = 0$. f_t is the tension force through the cadherin spring and f_{t-thr} is a force threshold.

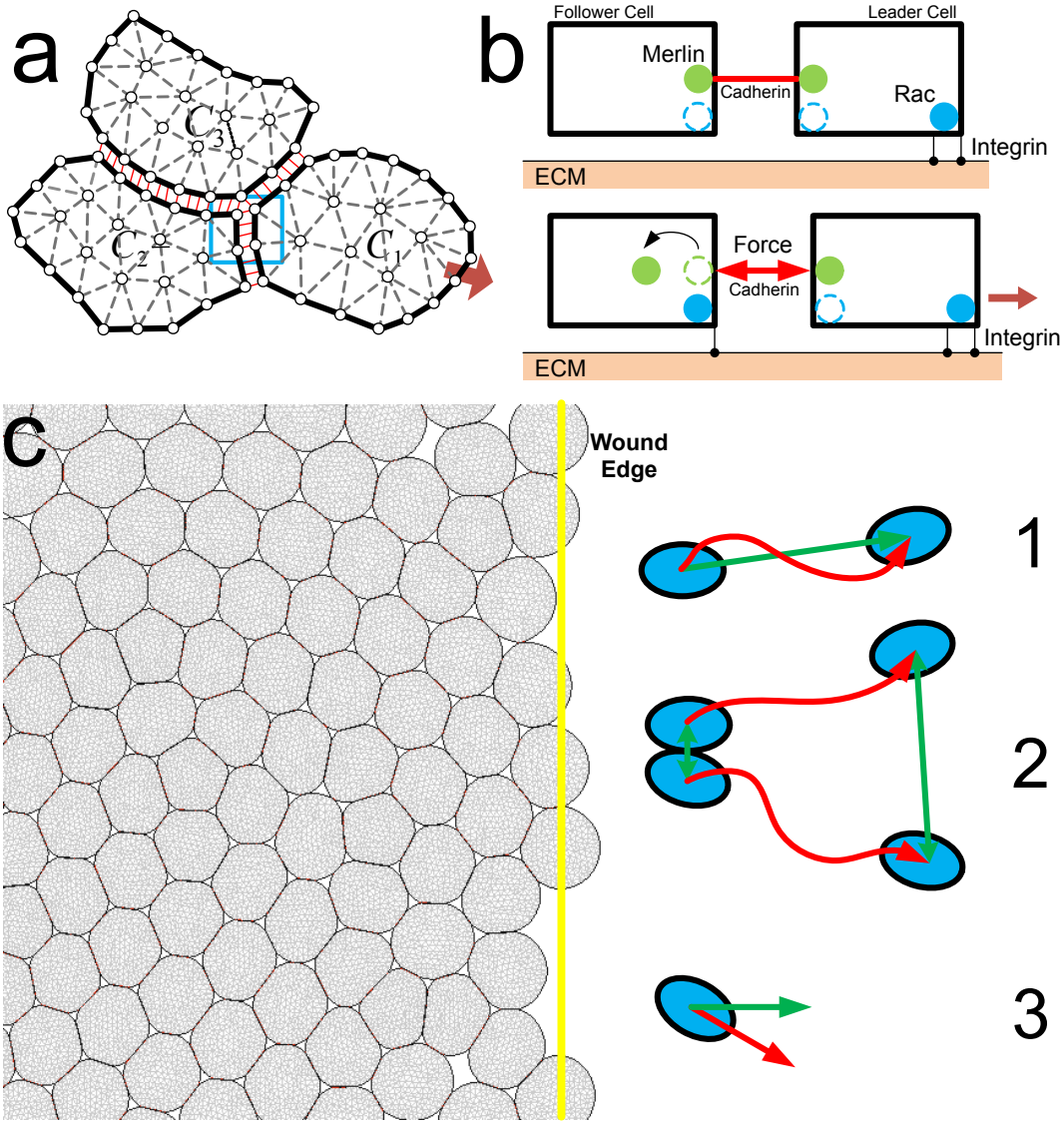

Fig. 2 Mechanosensing through intercellular adhesion and tissue structure for collective cell migration. (a) The intercellular adhesion, namely the cadherin spring (red springs in the blue box) are responsible for the transition of mechanical stimulus from leader cell (C_1) to follower cells (C_2 and C_3). (b) At static state, Merlin (to inhibit the Rac activation) is bound on the two ends of the cadherin spring. If there is stretch of the cadherin spring due to migration of leader cell, Merlin on the follower cell is delocated. Therefore, Rac can be activated on the follower cell. (c) The size of the wound tissue consisting of epithelial cells is $720\mu m \times 240\ \mu m$. The right side of the tissue boundary is set as the wound edge (yellow line). Cells can migrate to the open space on the right. There are three measurements to measure the collective cell migration: (1) Migration persistence $p(t_n)$ is the ratio of the distance from the current position of the cell at time t_n to its original position (green line) divided by the length of the traversed path (red curve); (2) Normalized pair separation distance $d_{i,j}(t_n)$ is the separation distance between a pair of cells at time t_n which were initially neighbors (green lines) normalized by the average length of cell traversed path (red curves); (3) Migration direction angle $\alpha(t_n)$ is the angle between the direction of cell migration (red arrow) and the direction to the wound (green arrow).

2.4 Structure of the cellular tissue for collective cell migration

In our model, the collective cell migration was simulated using a wound tissue consisting of epithelial cells. The tissue size is set to $720\mu m \times 240\ \mu m$. For comparison, we used the same type of epithelial cell, MCF-10A, used in the *in vitro* study (Ng et al., 2012). The corresponding epithelial-specific parameters is listed in Table 1 in Supplementary Information. We arbitrarily set the right side of the tissue boundary as the wound edge, and cells can migrate into the open space to the right of the wound edge (Fig. 2c). The mechano-chemical pathway was triggered first in the cells on the wound edge when they start to move. We followed a previous study (Ng et al., 2012) to divide the location of cells into four re-

gions according to their distance to the wound edge: Regions I, II, III, and IV have distance 0–160 μm, 160–320 μm, 320–480 μm, and 480–640 μm to the wound edge, respectively (Fig. 2c). The simulation was running for 12 biological hours, which is also the same experimental duration in the *in vitro* study (Ng et al., 2012).

2.5 Measurements of the collective cell migration

In our model, the collective cell migration are measured by the four measurements following (Ng et al., 2012):

The migration persistence. At time step t_n, the length of the straight line between cell positions at t_n and initial step t_0 over the length of the migration trajectory:

$$p(t_n) = \frac{|\boldsymbol{x}(t_n) - \boldsymbol{x}(t_0)|}{\sum_{k=0}^{n-1} |\boldsymbol{x}(t_{k+1}) - \boldsymbol{x}(t_k)|}, \tag{20}$$

where t_0 is the initial time, $\boldsymbol{x}(t_i)$ is the position of cell at time step t_i. The larger $p(t_n)$ is, the more persistent the cell migration is (Fig. 2c.1).

The normalized separation distance. At time step t_n, the separation distance of a pair of two neighboring cells 1-2, normalized by the average length of their migration trajectories:

$$d_{1,2}(t_i) = \frac{||\boldsymbol{x}_1(t_i) - \boldsymbol{x}_2(t_i)| - |\boldsymbol{x}_1(t_0) - \boldsymbol{x}_2(t_0)||}{\frac{1}{2}(\sum_{k=0}^{i-1} |\boldsymbol{x}_1(t_{k+1}) - \boldsymbol{x}_1(t_k)| + \sum_{k=0}^{i-1} |\boldsymbol{x}_2(t_{k+1}) - \boldsymbol{x}_2(t_k)|)}, \tag{21}$$

where the numerator measures the separation distance between cells i and j at time t_n, and the denominator measures the averaged path length of cells i and j at time t_n. The smaller $d_{i,j}(t_n)$ is, the better collective cell-cell coordination for this pair of cells is during cell migration (Fig. 2c.2).

The direction angle. The angle between the cell migration direction and the direction to the wound:

$$\alpha(t_n) = \arccos(\boldsymbol{u}_c \cdot \boldsymbol{u}_w) \cdot \mathrm{sgn}(\| \boldsymbol{u}_c \times \boldsymbol{u}_w \|), \tag{22}$$

where $\boldsymbol{u}_c$ is the unit vector of the direction of cell migration, $\boldsymbol{u}_w$ is the unit vector of direction from the cell mass center to the wound which is actually always $(1, 0)$, $\mathrm{sgn}(x)$ is the sign of x. The smaller $\alpha(t_n)$ is, the more accurate the migration direction is (Fig. 2c.3).

3 Results

3.1 Mechanics of cell-substrate is key to regulation of collective cell migration

3.1.1 Morphology and migration pattern under different substrate stiffness

We fist studied the process of collective cell migration of the wound tissue under the modeling mechano-chemical mechanism. Simulated cell trajectories showed that cells on stiffer substrate migrate faster and more persistently (Fig. 3a and 3b, Videos 1–2 in supplementary Information). This is consistent with *in vitro* observation of collective cell migration, which has shown the same pattern (Fig. 3c and 3d). In addition, the shape of individual cell also varied with substrate stiffness. Cells on softer substrate adopted a more spherical shape (Fig. 4a). In contrast, cells on stiffer substrate were more elongated (Fig. 4c). This pattern of cell morphology was also observed in (Ng et al., 2012), where cell on softer substrate extended its protrusions all around its boundary (Fig. 4b), while cell on stiffer substrate protruded only on the narrow leading side and left a long tail (Fig. 4d).

Overall, our simulated patterns of cell trajectory and cell morphology are consistent with that observed *in vitro*, indicating the validation of our mechano-chemical model is valid.

3.1.2 The mechanical signal has long-distance effects in guiding collective cell migration

We then quantified the cell migration process in more details to explore how mechanics of cell-substrate and cell-cell mechanics influence the collective cell migration using the measurements of persistent ratio $p(t_n)$, normalized separation distance $d_{i,j}(t_n)$ and direction angle $\alpha(t_n)$.

We first examined the migration speed of the cells. Generally, cells on stiffer substrate migrate with higher speed (Fig. 5a, more details of cell migration speed can be found in supplementary Information). In addition, on both stiffer and softer substrate, cells close to the wound edge migrated with the highest speed and this speed decreased gradually as the distance between cell and wound edge increased. On substrate at stiffness of 65 kPa, the migration speed decreased gradually from $0.69 \pm 0.01 \mu m/min$ in Region I to $0.49 \pm 0.02 \mu m/min$ in Region IV, while on substrate at stiffness of 3 kPa, the migration speed decreased gradually from $0.38 \pm 0.02 \mu m/min$ in Region I to $0.25 \pm 0.02 \mu m/min$ in Region IV (Fig. 5a). Our simulated cell

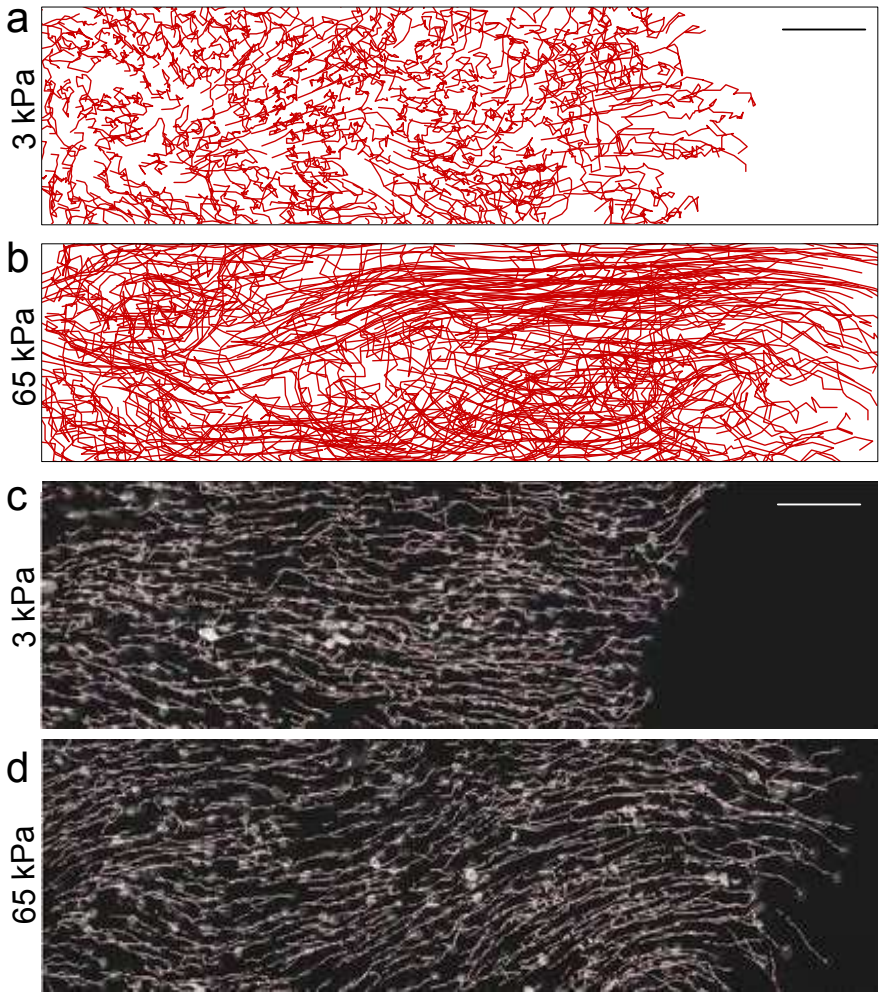

Fig. 3 Cell migration trajectories during collective cell migration. (a–b) The cell migration trajectory of our simulation using two substrate stiffness: 3 and 65 kPa. (c–d) The cell trajectory of the *in vitro* study using two substrate stiffness: 3 and 65 kPa (Ng et al., 2012). The scale bar: 100 μm. Copyright of (c–d): © 2012 Ng, et al. Originally published in Journal of Cell Biology: `https://doi.org/10.1083/jcb.201207148`.

migration speed was consistent with that reported in the *in vitro* study (Ng et al., 2012). It is easy to understand such a pattern of cell migration speed in different regions. For cells in Region I, especially on the leading edge, there are much fewer or no cells ahead. As the distance to the wound edge increased, it was more and more crowded for cells to migrate forward.

We then examined the migration persistence of the cells. As shown in Fig. 5b, cells on stiffer substrate migrate more persistently. In addition, cells close to the wound edge migrated with higher persistence than those far from the wound edge. For cells on substrate at stiffness of 65 kPa, the persistence ratio decreased from $82 \pm 2\%$ in Region I to $58 \pm 3\%$ in Region IV, while on substrate at stiffness of 3 kPa, the persistence ratio decreased from $71 \pm 1\%$ in Region I to $55 \pm 3\%$ in Region IV (Fig. 5b). As shown in Fig. 5c, cells on stiffer substrate migrate with better collective cell-cell coordination.

In addition, we examined the normalized separation distance of the cells. As shown in Fig. 5c, the normalized separation distance increased as the distance between cell and the wound edge increased. In our simulation, for cells on substrate at stiffness of 65 kPa, the separation distance decreased from 0.15 ± 0.02 in Region I to 0.11 ± 0.02 in Region II and then increased to 0.21 ± 0.03 in Region IV, while on substrate at stiffness of 3 kPa, the separation distance decreased from 0.22 ± 0.02 in Region I to 0.17 ± 0.02 in Region II and then increased to 0.19 ± 0.04 in Region IV (Fig. 5c). Our simulated separation distance was also similar to that reported in the *in vitro* study (Ng et al., 2012).

Furthermore, we examined the migration direction angle. We compared this measurement for cells on the leading edge of the wound tissue and cells 500 μm away

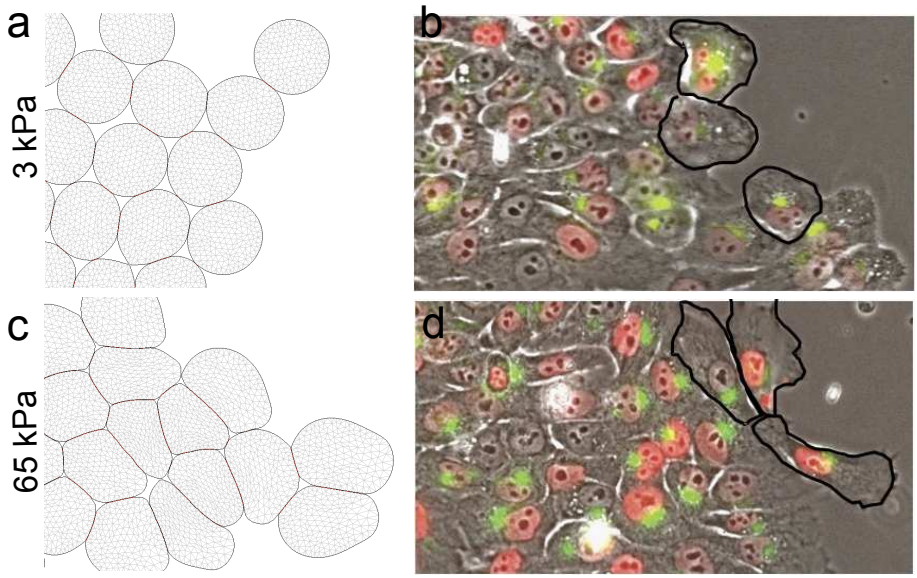

Fig. 4 Cell morphology during collective cell migration. (a,c) The cell morphology of our simulation using two substrate stiffness: 3 and 65 kPa. (b,d) The cell morphology of the *in vitro* study (Ng et al., 2012) using two substrate stiffness: 3 and 65 kPa. The cell boundary is highlighted in black. Copyright of (b) and (d): © 2012 Ng, et al. Originally published in Journal of Cell Biology: `https://doi.org/10.1083/jcb.201207148`.

from the wound edge. Since the migration direction is typically in the direction of the polarity axis (Rappel and Edelstein-Keshet, 2017), we also compared this direction angle to the polarization direction reported in a *in vitro* study (Ng et al., 2012). As shown in Fig. 5d–5g, cells on stiffer substrate (65 kPa) had more accurate migration direction towards the wound, even when they were far away from the wound edge (>500 μm). Only 10% of the cells on leading edge had migration direction opposite to the wound direction (Fig. 5d, 90°–270°), while this increased to 30% for cells >500 μm away from the wound edge (Fig. 5f, 90°–270°). However, for cells on softer substrate (3 kPa), migration direction deviated more from the direction towards the wound: 35% of the cells on leading edge had migration direction opposite to the wound direction (Fig. 5e, 90°–270°), while this increased to 45% for cells >500 μm away from the wound edge (Fig. 5g, 90°–270°).

As reflected from these measurements, substrate stiffness plays an important role in guiding collective cell migration with high persistence efficiently, good coordination between cells, and more accurate migration direction. Our simulation suggests that this was achieved due to the mechano-chemical feedback loop in each cell, which helped to dictate its own movement. However, these individual movements were eventually organized into a global migrative wave. This indicated that a simple and effective strategy based on individual cell can direct the migration of a large group of cells efficiently.

3.2 Influence of disrupted intercellular adhesions on collective cell migration

We have shown that the cell-substrate contact played key roles in guiding efficient collective cell migration. Our model shows that the transmission of such guidance cue was through the intercellular adhesions. Previous study has also provided evidence that mechanical tension are transmitted through cadherin between neighboring cells in response to external mechanical stimulus (Tambe et al., 2011). We further explored how the disruption of the intercellular adhesion can impact the collective cell migration. We modeled the disruption under two different assumptions. We examined the effects of these two models separately, and then their combinational effects. The effects of each case were then compared to the *in vitro* study (Ng et al., 2012).

3.2.1 Disruptions of the intercellular adhesion

We first introduced two models of disruption of the intercellular adhesions.

Model One: We first reduced cadherin's adhesive intensity, so cells were more easily to depart from each other. We decreased the adhesive intensity of the intercellular adhesion by reducing the spring constant of the cadherin springs between cells from 3.0 $nN/\mu m$ to 0.3 $nN/\mu m$.

Model Two: We perturbed the Merlin-delocation mechanism and examined the effects of reduced Merlin phosphorylation on the intercellular adhesion site due

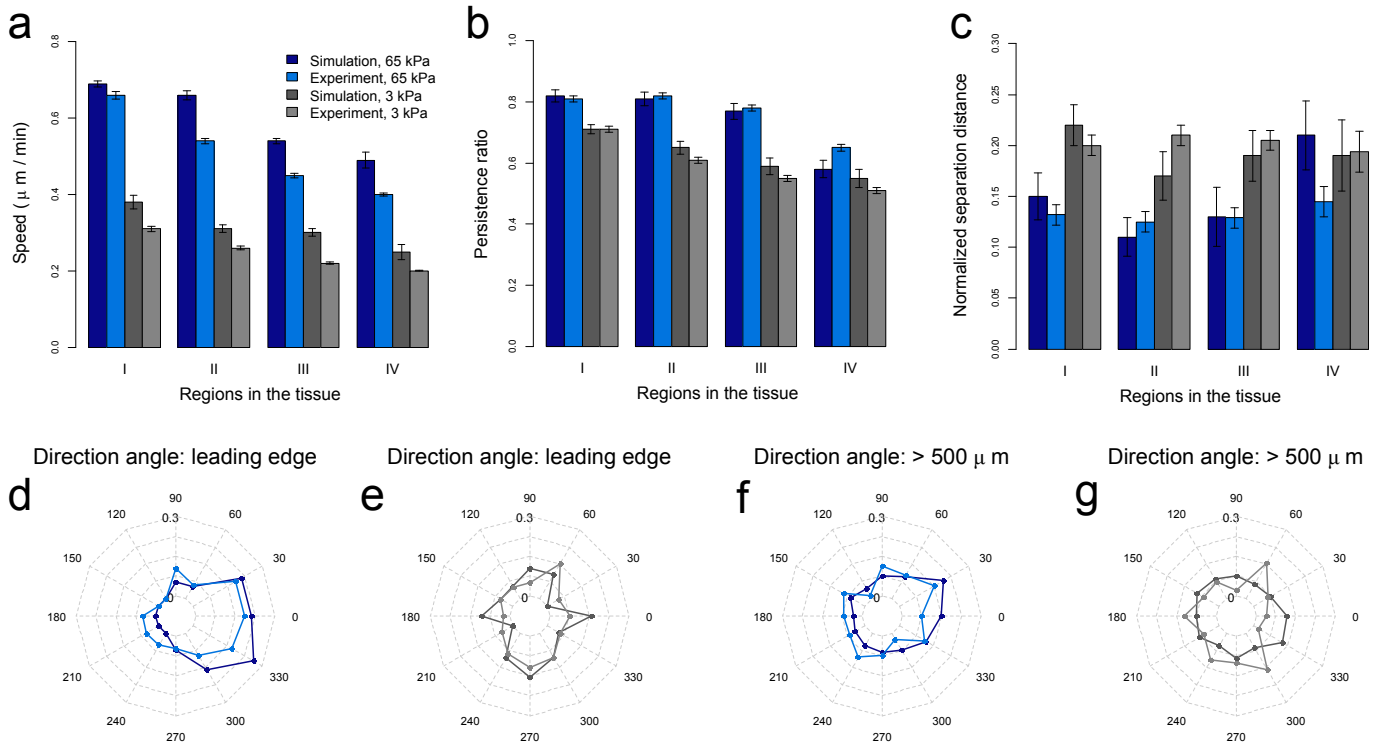

Fig. 5 Measurements to analyze the collective cell migration. (a–c) The cell migration speed, persistence ratio and normalized separation distance of our simulated wound tissue and the wound healing tissue in the *in vitro* study (Ng et al., 2012). (d–g) The migration direction angle of the cells on the leading edge and more than 500 μm from the wound edge in our simulation and the polarization direction angle of the cells on the leading edge and more than 500 μm from the wound edge in the *in vitro* study (Ng et al., 2012) on the substrate with stiffness 65 kPa (d–e) and 3 kPa (f–g). The colors indicating simulation or experiment are shown in (a). The error bars of our simulation depict the standard deviations of four simulation runs. The number of the experiments to create their error bars can be found in (Ng et al., 2012).

to the tension force generated on the cadherin spring. To model this effect, we decrease the value of k_p in Eqns 18 and 19 by 10-fold. With this perturbation, there is more activated Merlin on the sites of cell-cell contact. Since activated Merlin inhibits the formation of integrin, as a consequence, the ability of submarginal cell to follow leading cell will be altered.

The key difference between these two models is that **Model One** explores the effect of physical contact between cells while **Model Two** explores the effect of chemical signal transition between cells.

3.2.2 Effects of different models of disruption of the intercellular adhesion

Under both models of disruptions, the cell migration speed increased on both stiff and soft substrates. However, the degree of the increase under Model One was larger (Fig. 6a). The migration persistence decreased on both stiff and soft substrates, with the degree of decrease under Model Two larger (Fig. 6b). The normalized separation distance between migrating cells increased on both stiff and soft substrates. However, the degree of the increase under Model One was larger (Fig. 6c). These results indicated that reduced adhesive intensity of the intercellular adhesion has a stronger influence on cell-cell coordination, while reduced ability for cells to follow the leader cell through intercellular adhesion has a larger influence on cell migration persistence.

While these two models can be studied separated in our simulations, in real cells their effects may not be separable. To better understand which effect would be affected *in vitro*, we further compared our results to a *in vitro* study, where the cadherin activity was knocked down by treatment of siCDH3 (Ng et al., 2012). The degree of the decrease of persistence ratio observed *in vitro* (Ng et al., 2012) can be reproduced only when both models of disruptions were applied at the same time (Fig. 6b). This was also the case for the measurement of normalized separation distance. As shown in Fig. 6c, the degree of the increase of normalized separation distance can be roughly reproduced when both models were applied at the same time. Therefore, these results suggest that while cadherin activity is knocked down, both adhesive intensity and submarginal cell's ability to follow the migrative wave are affected *in vitro*.

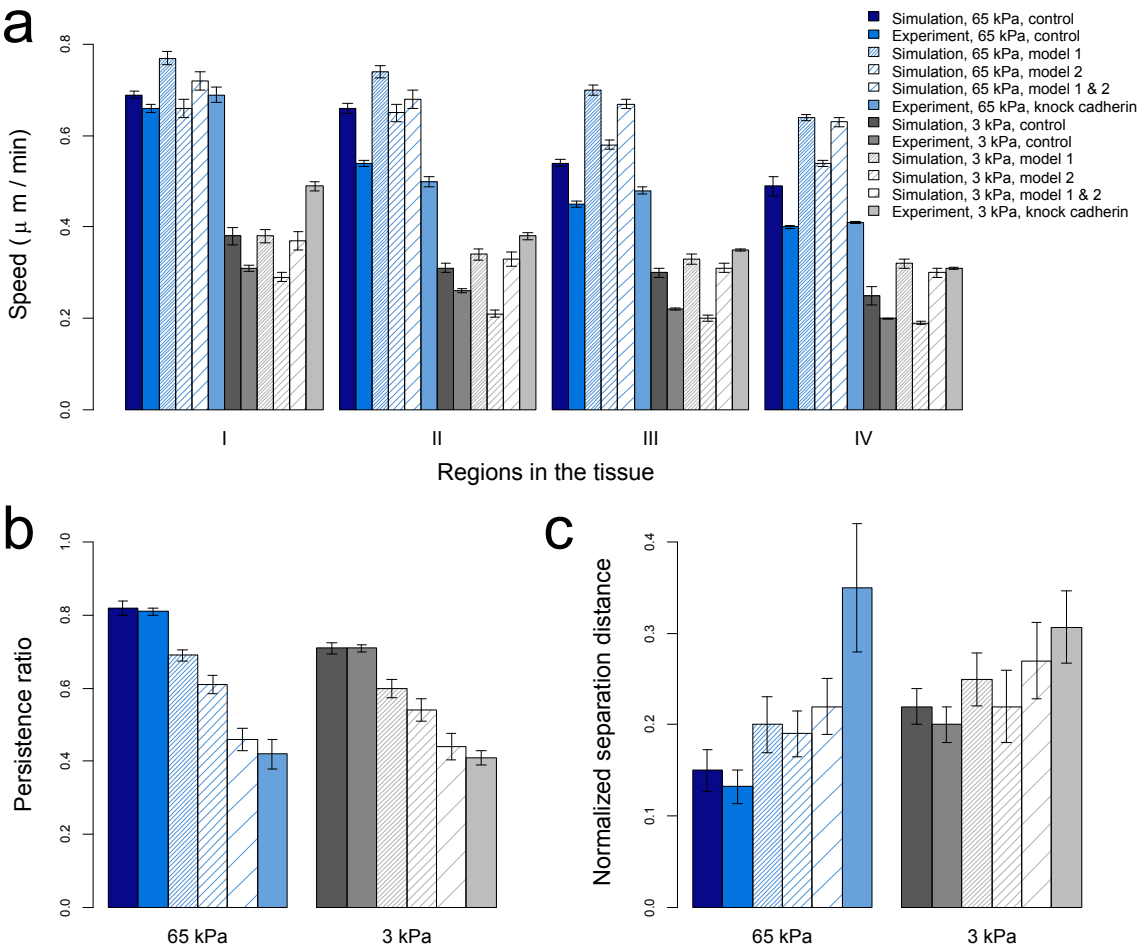

Fig. 6 Measurements to analyze the collective cell migration upon disrupted intercellular adhesion. The cell migration speed (a), persistence ratio (b) and normalized separation distance (c) of our simulated wound tissue under two models of disrupted intercellular adhesion and the wound healing tissue after knocking down cadherin in the *in vitro* study (Ng et al., 2012). The error bars of our simulation depict the standard deviations of four simulation runs. The number of the experiments to create their error bars can be found in (Ng et al., 2012).

Additional support for our conclusion comes from the measurement of migration direction angle. As shown in Fig. 7a–7d, there were more cell migration direction angle distributed in the region 330°–30° under Model Two when compared to that under Model One. The migration direction angle under Model One was more evenly distributed in all directions. This might indicate that under Model Two, even when the ability for the follower cell to protrude with the leader cell was reduced, the intercellular adhesion can still transmit guidance cue for the follower cell if two cells come into contact, which enables the correct migration direction. We also found that the distribution of migration direction angle matches with the distribution of polarization direction of the cells with blocked cadherin (Ng et al., 2012) better when both scenario occurred at the same time. This might suggest that both modes of disruptions may occur when cadherin is impeded *in vitro*.

4 Discussion

Collective cell migration is an essential process that enables coordination of movement of group of cells, while ensuring that they remain connected through intercellular adhesions. However, our understanding of the mechanisms of collective cell migration in a complex mechanical environment still remains limited (Li et al., 2015). A number of computational cell models have been developed to explore the effects of different cellular mechanics on collective cell migration, each with its limitations.

In this study, we developed a novel finite element cellular model to explain the mechanism behind collective cell migration using a simplified wound tissue model. The model includes a detailed mechano-chemical feedback loop, which takes into account of focal adhesion formation and cell protrusion triggered by Rac signaling, which is activated by focal adhesion. In ad-

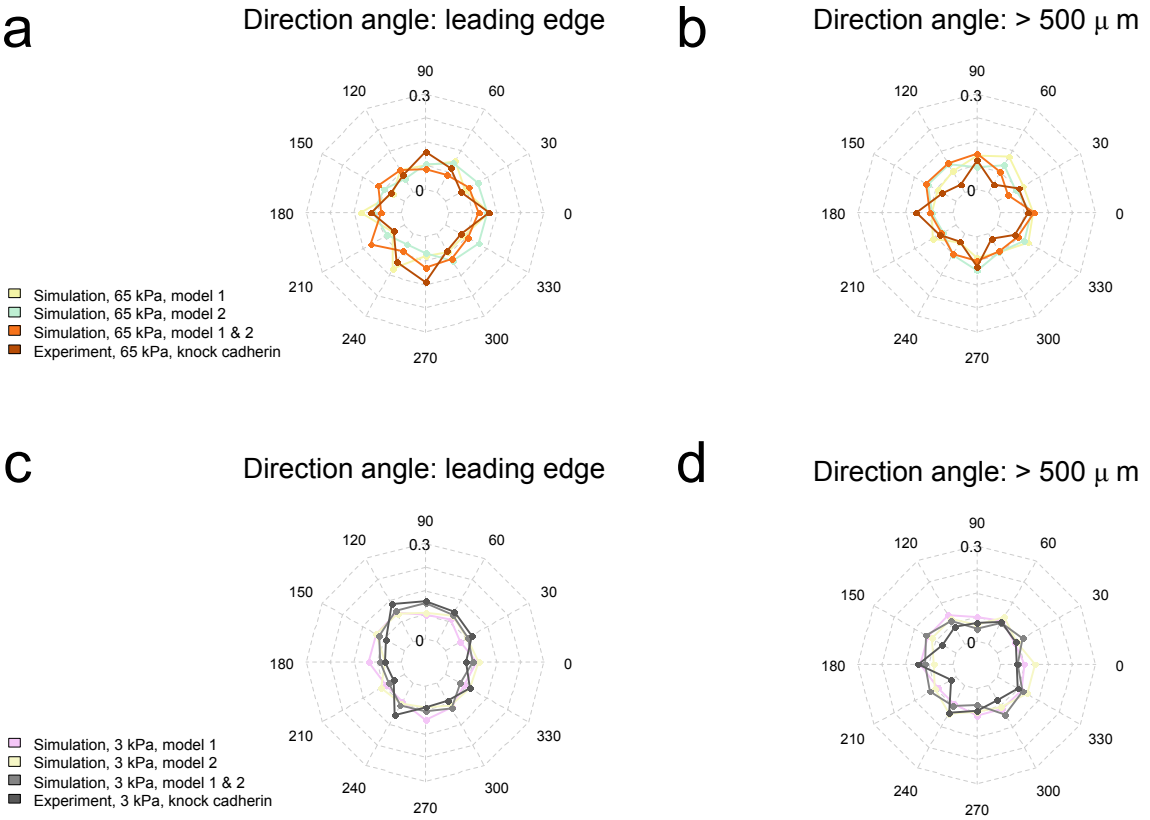

Fig. 7 The migration angle of the cells upon disrupted intercellular adhesion. (a–d) The migration direction angle of the cells on the leading edge and more than 500 μm from the wound edge in our simulation under the two models of disrupting the intercellular adhesion and the polarization direction angle of the cells on the leading edge and more than 500 μm from the wound edge in the *in vitro* study after knocking down cadherin (Ng et al., 2012).

dition, our model also incorporates the mechanical cue guiding the follower cell to follow the leader cell, which is triggered by the mechanical force generated on intercellular adhesions. We specifically examine the effects of cell-substrate contact and intercellular adhesions on collective cell migration during wound healing process.

An important result of this study is that we find the cell-substrate mechanics plays key role in guiding directed and persistent collective cell migration. Stiffer substrate has better guidance of the collective cell migration, with more accurate direction, higher persistence , and better cell-cell coordination (Fig. 5). Previous *in vitro* study has shown that cells on stiffer substrate tend to have elongated shape while cells on softer substrate tend to have spherical shape (Ansardamavandi et al., 2018). Our simulation shows the same pattern of cell morphology varied with substrate stiffness (Fig. 4a and 4c). One possible explanation could be that cells with elongated shape have larger traction force exerted on the leading edge, which is much narrower compared to cells with spherical shape. Therefore, the Rac-mediated protrusion on elongated cell would be more persistent. Recent study on the cell-substrate contact guidance also showed that the biased spatial distribution of focal adhesion enhanced the directed migration (Ramirez-San Juan et al., 2017). Our mechanochemical model suggested that the larger focal adhesion on stiffer substrate promoted the Rac-mediated cell protrusion and cell elongation, which in turn enhanced the formation and maintenance of focal adhesion on the leading edge.

Our simulation further demonstrated that intercellular adhesion functions cooperatively to maintain persistent migration for all cells in the group. The basic function of intercellular adhesions is to maintain tissue integrity during collective migration (Vedula et al., 2014). Recent study has also shown additional functions of cadherin adhesion. It supresses the Rac activity, preventing two cells in contact to intrude each other (Okada et al., 2005). On the other hand, the stretching force on cadherin triggers Merlin-Tiam1 related pathway to initiate Rac activity again to ensure cells behind the leading migrating cells to follow (Venhuizen and Zegers, 2017).

Our simulation shows that these two functions of the intercellular adhesion enhance the maintenance of

the migration direction of the submarginal cells to join and follow the migrative wave. The intercellular adhesions between cells in the same row of the migrative wave result in a contact-inhibition effect, which enhances the cell's protrusion only on the leading edge, while the intercellular adhesions between pairs of cells in leader-follower relationship promote the follower cell to protrude to follow the leader cell (as shown in Fig. 2b and Fig.1 in supplementary Information). Through this mechanism, the migration direction can be maintained in long distance: even for cells 500 μm away from the front row of cells in the tissue, they maintain the correct migration direction (Fig. 5d–5g).

Upon disruptions of the adhesive intensity of the intercellular adhesion, cell-cell coordination during collective migration was perturbed (Fig. 6c). Upon disruption of cell's ability to sense mechanical changes on the intercellular adhesion to protrude with the leader cell, the cell migration persistence was reduced (Fig. 6b). The migration direction angle was also disturbed as consequence of disrupted intercellular adhesion that cells are unable to find the correct migration direction (Fig. 7a–7d).

In our model, the protein in cadherin-mediated pathway regulating the transmission of the mechanical cue is taken as Merlin following (Das et al., 2015). There are also other proteins performing similar function of transmitting mechanical signal. Previous study reported that cells with depleted αE-catenin migrated more randomly (Benjamin et al., 2010). The activation of $\alpha 7$ subunits of nAChRs, which is responsible for signal transmission enhanced the directional migration and inhibited random migration of keratinocyte (Chernyavsky et al., 2004). Our simulation together with these studies suggested that the need for a category of proteins regulating the intercellular adhesion. They are not necessarily one specific type of protein, so long as they function as a mechanical sensor to transmit the mechanical cue, so the overall migration direction of the collective cell migration is maintained.

In addition, by comparing the measurements of persistence ratio, normalized separation distance, and migration direction angle between our simulation and the observation in the *in vitro* study (Ng et al., 2012), our results suggested that upon removal of cadherin activity, both effects of adhesive intensity and transmission of the directional cue through the intercellular adhesion are affected. Our computational model provides means to focus on a single factor and examine its specific effects in details. This would be difficult to achieve in an experimental study, as it is too complicated to manipulate single factor, due to their interdependency on each other.

There are a number of limitations of our cellular finite element model. First, the influence of substrate stiffness on cell is largely focused on cell mechanics in our model. Previous experimental and theoretical studies have provided insight into how the mechanical cues are translated into biochemical signals through a mechanically-sensitive clutch mechanism at the single cell level (MacDonald et al., 2008; Welf et al., 2013). The molecular clutches link F-actin to the substrate and mechanically resist myosin-driven F-actin retrograde flow (Chan and Odde, 2008), which is a fundamental regulator of traction force at focal adhesions during cell migration (Gardel et al., 2008). To better reproduce the cell migration speed, the effect of this clutch mechanism should be considered. Second, the simplified cell-cell adhesion in our model is independent of the traction force between cell and substrate and cell behavior. Previous experimental studies showed that changes of cell protrusion and cell tractions result in modulation of endogenous tension and force redistribution in cell-cell contact (Maruthamuthu et al., 2011; Maruthamuthu and Gardel, 2014). These findings indicate that there is more complex mechanism behind cadherin-based intercellular adhesions. A more comprehensive cell-cell adhesion model needs to be developed to capture these experimental observations.

In summary, our finite element cellular model demonstrated that the cell-substrate mechanics plays important role in guiding collective cell migration with high efficiency. This guidance cue is maintained and transmitted to cells within the tissue by intercellular adhesions. We anticipate that our model can be applied to studies of additional cellular tissue problems.

Conflicts of interest

The authors declare that they have no conflict of interest.

Acknowledgements This study was supported by the funding from National Institutes of Health (NIH): R01 CA204962, R35 GM127084. We thank Dr. Joan S. Brugge, Dr. Gaudenz Danuser, and Dr. Mei Rosa Ng to grant the permission to use their published experimental data (Fig. 3c, 3d and Fig. 4b, 4d).

References

Albert, P. J. and Schwarz, U. S. (2016), Dynamics of cell ensembles on adhesive micropatterns: bridging the gap between single cell spreading and collective cell migration, *PLoS computational biol-*

ogy **12**(4), e1004863. https://doi.org/10.1371/journal.pcbi.1004863

Alberts, B. (2008), *Molecular Biology of the Cell: Reference edition*, number v. 1 *in* Molecular Biology of the Cell: Reference Edition, Garland Science.

Ansardamavandi, A., Tafazzoli-Shadpour, M. and Shokrgozar, M. A. (2018), Behavioral remodeling of normal and cancerous epithelial cell lines with differing invasion potential induced by substrate elastic modulus, *Cell adhesion & migration* **12**(5), 472–488. https://doi.org/10.1080/19336918.2018.1475803

Banerjee, S. and Marchetti, M. C. (2012), Contractile stresses in cohesive cell layers on finite-thickness substrates, *Physical review letters* **109**(10), 108101. https://doi.org/10.1103/PhysRevLett.109.108101

Barnhart, E., Lee, K.-C., Keren, K., Mogilner, A. and Theriot, J. (2011), An adhesion-dependent switch between mechanisms that determine motile cell shape, *PLoS Biol* **9**(5), e1001059. https://doi.org/10.1371/journal.pbio.1001059

Basan, M., Elgeti, J., Hannezo, E., Rappel, W.-J. and Levine, H. (2013), Alignment of cellular motility forces with tissue flow as a mechanism for efficient wound healing, *Proceedings of the National Academy of Sciences* **110**(7), 2452–2459. https://doi.org/10.1073/pnas.1219937110

Benjamin, J. M., Kwiatkowski, A. V., Yang, C., Korobova, F., Pokutta, S., Svitkina, T., Weis, W. I. and Nelson, W. J. (2010), αE-catenin regulates actin dynamics independently of cadherin-mediated cell–cell adhesion, *The Journal of cell biology* **189**(2), 339–352. https://doi.org/10.1083/jcb.200910041

Brugués, A., Anon, E., Conte, V., Veldhuis, J. H., Gupta, M., Colombelli, J., Muñoz, J. J., Brodland, G. W., Ladoux, B. and Trepat, X. (2014), Forces driving epithelial wound healing, *Nature Physics* **10**(9), 683–690. https://doi.org/10.1038/nphys3040

Chan, C. E. and Odde, D. J. (2008), Traction dynamics of filopodia on compliant substrates, *Science* **322**(5908), 1687–1691. https://doi.org/10.1126/science.1163595

Changede, R. and Sheetz, M. (2017), Integrin and cadherin clusters: A robust way to organize adhesions for cell mechanics, *BioEssays* **39**(1), 1–12. https://doi.org/10.1002/bies.201600123

Checa, S., Rausch, M. K., Petersen, A., Kuhl, E. and Duda, G. N. (2015), The emergence of extracellular matrix mechanics and cell traction forces as important regulators of cellular self-organization, *Biomechanics and modeling in mechanobiology* **14**(1), 1–13. https://doi.org/10.1007/s10237-014-0581-9

Chernyavsky, A. I., Arredondo, J., Marubio, L. M. and Grando, S. A. (2004), Differential regulation of keratinocyte chemokinesis and chemotaxis through distinct nicotinic receptor subtypes, *Journal of cell science* **117**(23), 5665–5679. https://doi.org/10.1242/jcs.01492

Cirit, M., Krajcovic, M., Choi, C. K., Welf, E. S., Horwitz, A. F. and Haugh, J. M. (2010), Stochastic model of integrin-mediated signaling and adhesion dynamics at the leading edges of migrating cells, *PLoS Comput Biol* **6**(2), e1000688. https://doi.org/10.1371/journal.pcbi.1000688

Das, T., Safferling, K., Rausch, S., Grabe, N., Boehm, H. and Spatz, J. P. (2015), A molecular mechanotransduction pathway regulates collective migration of epithelial cells, *Nature cell biology* **17**(3), 276. https://doi.org/10.1038/ncb3115

Defranco, B. H., Nickel, B. M., Baty, C. J., Martinez, J. S., Gay, V. L., Sandulache, V. C., Hackam, D. J. and Murray, S. A. (2008), Migrating cells retain gap junction plaque structure and function, *Cell communication & adhesion* **15**(3), 273–288. https://doi.org/10.1080/15419060802198298

DiMilla, P., Barbee, K. and Lauffenburger, D. (1991), Mathematical model for the effects of adhesion and mechanics on cell migration speed., *Biophysical journal* **60**(1), 15. https://doi.org/10.1016/S0006-3495(91)82027-6

Dokukina, I. V. and Gracheva, M. E. (2010), A model of fibroblast motility on substrates with different rigidities, *Biophysical journal* **98**(12), 2794–2803. https://doi.org/10.1016/j.bpj.2010.03.026

Drasdo, D. and Hoehme, S. (2012), Modeling the impact of granular embedding media, and pulling versus pushing cells on growing cell clones, *New Journal of Physics* **14**(5), 055025. https://doi.org/10.1088/1367-2630/14/5/055025

Friedl, P. and Gilmour, D. (2009), Collective cell migration in morphogenesis, regeneration and cancer, *Nature reviews Molecular cell biology* **10**(7), 445–457. https://doi.org/10.1038/nrm2720

Gardel, M. L., Sabass, B., Ji, L., Danuser, G., and Schwarz, U. S. (2008), Traction stress in focal adhesions correlates biphasically with actin retrograde flow speed, *Journal of Cell Biology* **183**(6), 999–1005. https://doi.org/10.1083/jcb.200810060

Hoehme, S. and Drasdo, D. (2010), A cell-based simulation software for multi-cellular systems, *Bioinformatics* **26**(20), 2641–2642. https://doi.org/10.1093/bioinformatics/btq437

Holle, A. W. and Engler, A. J. (2011), More than a feeling: discovering, understanding, and influenc-

ing mechanosensing pathways, *Current opinion in biotechnology* **22**(5), 648–654. https://doi.org/10.1016/j.copbio.2011.04.007

Hu, S., Wang, R., Tsang, C. M., Tsao, S. W., Sun, D. and Lam, R. H. (2018), Revealing elasticity of largely deformed cells flowing along confining microchannels, *RSC advances* **8**(2), 1030–1038. https://doi.org/10.1039/C7RA10750A

Hutson, M. S., Veldhuis, J., Ma, X., Lynch, H. E., Cranston, P. G. and Brodland, G. W. (2009), Combining laser microsurgery and finite element modeling to assess cell-level epithelial mechanics, *Biophysical journal* **97**(12), 3075–3085. https://doi.org/10.1016/j.bpj.2009.09.034

Jamali, Y., Azimi, M. and Mofrad, M. R. (2010), A sub-cellular viscoelastic model for cell population mechanics, *PLoS One* **5**(8), e12097. https://doi.org/10.1371/journal.pone.0012097

Kabla, A. J. (2012), Collective cell migration: leadership, invasion and segregation, *Journal of The Royal Society Interface* p. rsif20120448. https://doi.org/10.1098/rsif.2012.0448

Kachalo, S., Naveed, H., Cao, Y., Zhao, J. and Liang, J. (2015), Mechanical model of geometric cell and topological algorithm for cell dynamics from single-cell to formation of monolayered tissues with pattern, *PloS one* **10**(5), e0126484. https://doi.org/10.1371/journal.pone.0126484

Karcher, H., Lammerding, J., Huang, H., Lee, R. T., Kamm, R. D. and Kaazempur-Mofrad, M. R. (2003), A three-dimensional viscoelastic model for cell deformation with experimental verification, *Biophysical journal* **85**(5), 3336–3349. https://doi.org/10.1016/S0006-3495(03)74753-5

Kim, J. H., Serra-Picamal, X., Tambe, D. T., Zhou, E. H., Park, C. Y., Sadati, M., Park, J.-A., Krishnan, R., Gweon, B., Millet, E. et al. (2013), Propulsion and navigation within the advancing monolayer sheet, *Nature materials* **12**(9), 856–863. https://doi.org/10.1038/nmat3689

Kim, M.-C., Silberberg, Y. R., Abeyaratne, R., Kamm, R. D. and Asada, H. H. (2018), Computational modeling of three-dimensional ecm-rigidity sensing to guide directed cell migration, *Proceedings of the National Academy of Sciences* p. 201717230. https://doi.org/10.1073/pnas.1717230115

Kim, M.-C., Whisler, J., Silberberg, Y. R., Kamm, R. D. and Asada, H. H. (2015), Cell invasion dynamics into a three dimensional extracellular matrix fibre network, *PLoS computational biology* **11**(10), e1004535. https://doi.org/10.1371/journal.pcbi.1004535

Ladoux, B., Mège, R.-M. and Trepat, X. (2016), Front–rear polarization by mechanical cues: From single cells to tissues, *Trends in cell biology* **26**(6), 420–433. https://doi.org/10.1016/j.tcb.2016.02.002

Lauffenburger, D. A. and Horwitz, A. F. (1996), Cell migration: a physically integrated molecular process, *Cell* **84**(3), 359–369. https://doi.org/10.1016/S0092-8674(00)81280-5

Lautscham, L. A., Kämmerer, C., Lange, J. R., Kolb, T., Mark, C., Schilling, A., Strissel, P. L., Strick, R., Gluth, C., Rowat, A. C. et al. (2015), Migration in confined 3D environments is determined by a combination of adhesiveness, nuclear volume, contractility, and cell stiffness, *Biophysical journal* **109**(5), 900–913. https://doi.org/10.1016/j.bpj.2015.07.025

Lee, P. and Wolgemuth, C. W. (2011), Crawling cells can close wounds without purse strings or signaling, *PLoS computational biology* **7**(3), e1002007. https://doi.org/10.1371/journal.pcbi.1002007

Lee, R. M., Yue, H., Rappel, W.-J. and Losert, W. (2017), Inferring single-cell behaviour from large-scale epithelial sheet migration patterns, *Journal of The Royal Society Interface* **14**(130), 20170147. https://doi.org/10.1098/rsif.2017.0147

Leong, C., Krishna, V., Lim, T. and Ladoux, B. (2013), Geometrical constraints and physical crowding direct collective migration of fibroblasts, *Communicative & integrative biology* **6**(2), e23197. https://doi.org/10.4161/cib.23197

Li, L., He, Y., Zhao, M. and Jiang, J. (2015), Collective cell migration: Implications for wound healing and cancer invasion, *Burns & Trauma* **1**(1), 21. https://doi.org/10.4103/2321-3868.113331

Li, Y., Bhimalapuram, P. and Dinner, A. R. (2010), Model for how retrograde actin flow regulates adhesion traction stresses, *Journal of Physics: Condensed Matter* **22**(19), 194113. https://doi.org/10.1088/0953-8984/22/19/194113

MacDonald, A., Horwitz, A. R. and Lauffenburger, D. A. (2008), Kinetic model for lamellipodal actin-integrin clutch dynamics, *Cell Adhesion & Migration* **2**(2), 95–105. https://doi.org/10.4161/cam.2.2.6210

Marée, A. F., Grieneisen, V. A. and Hogeweg, P. (2007), The cellular potts model and biophysical properties of cells, tissues and morphogenesis, *in* Single-cell-based models in biology and medicine, Springer, pp. 107–136. https://doi.org/10.1007/978-3-7643-8123-3_5

Maruthamuthu, V., Sabass, B., Schwarz, U. S. and Gardel, M. L. (2011), Cell-ECM traction force modulates endogenous tension at cell-cell contacts,

Proceedings of the National Academy of Sciences **108**(12), 4708–4713. https://doi.org/10.1073/pnas.1011123108

Maruthamuthu, V., and Gardel, M. L. (2014), Protrusive activity guides changes in cell-cell tension during epithelial cell scattering, *Biophysical Journal* **107**(3), 555–563. https://doi.org/10.1016/j.bpj.2014.06.028

Merchant, B., Edelstein-Keshet, L. and Feng, J. J. (2018), A rho-gtpase based model explains spontaneous collective migration of neural crest cell clusters, *Developmental biology* **444**, S262–S273. https://doi.org/10.1016/j.ydbio.2018.01.013

Nagai, T. and Honda, H. (2009), Computer simulation of wound closure in epithelial tissues: Cell–basal-lamina adhesion, *Physical Review E* **80**(6), 061903. https://doi.org/10.1103/PhysRevE.80.061903

Nematbakhsh, A., Sun, W., Brodskiy, P. A., Amiri, A., Narciso, C., Xu, Z., Zartman, J. J. and Alber, M. (2017), Multi-scale computational study of the mechanical regulation of cell mitotic rounding in epithelia, *PLoS computational biology* **13**(5), e1005533. https://doi.org/10.1371/journal.pcbi.1005533

Ng, M. R., Besser, A., Danuser, G. and Brugge, J. S. (2012), Substrate stiffness regulates cadherin-dependent collective migration through myosin-ii contractility, *The Journal of cell biology* **199**(3), 545–563. https://doi.org/10.1083/jcb.201207148

Nikkhah, M., Edalat, F., Manoucheri, S. and Khademhosseini, A. (2012), Engineering microscale topographies to control the cell–substrate interface, *Biomaterials* **33**(21), 5230–5246. https://doi.org/10.1016/j.biomaterials.2012.03.079

Oakes, P., Banerje, S., Marchetti, M. and Gardel, M. (2014), Geometry regulates traction stresses in adherent cells, *Biophysical Journal* **107**, 825–833. https://doi.org/10.1016/j.bpj.2014.06.045

Okada, T., Lopez-Lago, M. and Giancotti, F. G. (2005), Merlin/nf-2 mediates contact inhibition of growth by suppressing recruitment of rac to the plasma membrane, *J Cell Biol* **171**(2), 361–371. https://doi.org/10.1083/jcb.200503165

Ramirez-San Juan, G., Oakes, P. and Gardel, M. (2017), Contact guidance requires spatial control of leading-edge protrusion, *Molecular biology of the cell* **28**(8), 1043–1053. https://doi.org/10.1091/mbc.e16-11-0769

Rape, A. D., Guo, W.-h. and Wang, Y.-l. (2011), The regulation of traction force in relation to cell shape and focal adhesions, *Biomaterials* **32**(8), 2043–2051. https://doi.org/10.1016/j.biomaterials.2010.11.044

Rappel, W.-J. and Edelstein-Keshet, L. (2017), Mechanisms of cell polarization, *Current opinion in systems biology* **3**, 43–53. https://doi.org/10.1016/j.coisb.2017.03.005

Ridley, A. J., Schwartz, M. A., Burridge, K., Firtel, R. A., Ginsberg, M. H., Borisy, G., Parsons, J. T. and Horwitz, A. R. (2003), Cell migration: integrating signals from front to back, *Science* **302**(5651), 1704–1709. https://doi.org/10.1126/science.1092053

Rørth, P. (2007), Collective guidance of collective cell migration, *Trends in Cell Biology* **17**(12), 575–579. https://doi.org/10.1016/j.tcb.2007.09.007

Rubinstein, B., Fournier, M. F., Jacobson, K., Verkhovsky, A. B. and Mogilner, A. (2009), Actin-myosin viscoelastic flow in the keratocyte lamellipod, *Biophysical Journal* **97**(7), 1853–1863. https://doi.org/10.1016/j.bpj.2009.07.020

Sandersius, S., Weijer, C. and Newman, T. (2011), Emergent cell and tissue dynamics from subcellular modeling of active biomechanical processes, *Physical Biology* **8**(4), 045007. https://doi.org/10.1088/1478-3975/8/4/045007

Schoner, J. L., Lang, J. and Seidel, H.-P. (2004), Measurement-based interactive simulation of viscoelastic solids, *in* 'Computer Graphics Forum', Vol. 23, Wiley Online Library, pp. 547–556. https://doi.org/10.1111/j.1467-8659.2004.00786.x

Schwartz, J.-M., Denninger, M., Rancourt, D., Moisan, C. and Laurendeau, D. (2005), Modelling liver tissue properties using a non-linear visco-elastic model for surgery simulation, *Medical Image Analysis* **9**(2), 103–112. https://doi.org/10.1016/j.media.2004.11.002

Sedef, M., Samur, E. and Basdogan, C. (2006), Real-time finite-element simulation of linear viscoelastic tissue behavior based on experimental data, *Computer Graphics and Applications, IEEE* **26**(6), 58–68. https://doi.org/10.1109/MCG.2006.135

Sheets, K., Wunsch, S., Ng, C. and Nain, A. S. (2013), Shape-dependent cell migration and focal adhesion organization on suspended and aligned nanofiber scaffolds, *Acta biomaterialia* **9**(7), 7169–7177. https://doi.org/10.1016/j.actbio.2013.03.042

Stéphanou, A., Mylona, E., Chaplain, M. and Tracqui, P. (2008), A computational model of cell migration coupling the growth of focal adhesions with oscillatory cell protrusions, *Journal of theoretical biology* **253**(4), 701–716. https://doi.org/10.1016/j.jtbi.2008.04.035

Tambe, D. T., Hardin, C. C., Angelini, T. E., Rajendran, K., Park, C. Y., Serra-Picamal, X., Zhou, E. H., Zaman, M. H., Butler, J. P., Weitz, D. A. et al.

(2011), Collective cell guidance by cooperative intercellular forces, *Nature Materials* **10**(6), 469–475. https://doi.org/10.1038/nmat3025

Trepat, X., Wasserman, M. R., Angelini, T. E., Millet, E., Weitz, D. A., Butler, J. P. and Fredberg, J. J. (2009), Physical forces during collective cell migration, *Nature Physics* **5**(6), 426–430. https://doi.org/10.1038/nphys1269

Van Liedekerke, P., Neitsch, J., Johann, T., Alessandri, K., Nassoy, P. and Drasdo, D. (2019), Quantitative cell-based model predicts mechanical stress response of growing tumor spheroids over various growth conditions and cell lines, *PLoS computational biology* **15**(3), e1006273. https://doi.org/10.1371/journal.pcbi.1006273

Vedula, S. R. K., Hirata, H., Nai, M. H., Toyama, Y., Trepat, X., Lim, C. T., Ladoux, B. et al. (2014), Epithelial bridges maintain tissue integrity during collective cell migration, *Nature materials* **13**(1), 87. https://doi.org/10.1038/nmat3814

Venhuizen, J.-H. and Zegers, M. M. (2017), Making heads or tails of it: Cell–cell adhesion in cellular and supracellular polarity in collective migration, *Cold Spring Harbor perspectives in biology* **9**(11), a027854. https://doi.org/10.1101/cshperspect.a027854

Vermolen, F. and Gefen, A. (2015), Semi-stochastic cell-level computational modelling of cellular forces: application to contractures in burns and cyclic loading, *Biomechanics and modeling in mechanobiology* **14**(6), 1181–1195. https://doi.org/10.1007/s10237-015-0664-2

Vitorino, P., Hammer, M., Kim, J. and Meyer, T. (2011), A steering model of endothelial sheet migration recapitulates monolayer integrity and directed collective migration, *Molecular and Cellular Biology* **31**(2), 342–350. https://doi.org/10.1128/MCB.00800-10

Watt, F. M. and Green, H. (1981), Involucrin synthesis is correlated with cell size in human epidermal cultures., *The Journal of Cell Biology* **90**(3), 738–742. https://doi.org/10.1083/jcb.90.3.738

Watt, F. M. and Huck, W. T. (2013), Role of the extracellular matrix in regulating stem cell fate, *Nature reviews Molecular cell biology* **14**(8), 467–473. https://doi.org/10.1038/nrm3620

Weber, G. F., Bjerke, M. A. and DeSimone, D. W. (2012), A mechanoresponsive cadherin-keratin complex directs polarized protrusive behavior and collective cell migration, *Developmental Cell* **22**(1), 104–115. https://doi.org/10.1016/j.devcel.2011.10.013

Welf, E. S., Johnson, H. E. and Haugh, J. M. (2013), Bidirectional coupling between integrin-mediated signaling and actomyosin mechanics explains matrix-dependent intermittency of leading-edge motility, *Molecular Biology of the Cell* **24**(24), 3945–3955. https://doi.org/10.1091/mbc.E13-06-0311

Wolf, K., Te Lindert, M., Krause, M., Alexander, S., Te Riet, J., Willis, A. L., Hoffman, R. M., Figdor, C. G., Weiss, S. J. and Friedl, P. (2013), Physical limits of cell migration: control by ecm space and nuclear deformation and tuning by proteolysis and traction force, *J Cell Biol* **201**(7), 1069–1084. https://doi.org/10.1083/jcb.201210152

Wu, Y. I., Frey, D., Lungu, O. I., Jaehrig, A., Schlichting, I., Kuhlman, B. and Hahn, K. M. (2009), A genetically encoded photoactivatable rac controls the motility of living cells, *Nature* **461**(7260), 104–108. https://doi.org/10.1038/nature08241

Yeh, Y.-C., Ling, J.-Y., Chen, W.-C., Lin, H.-H. and Tang, M.-J. (2017), Mechanotransduction of matrix stiffness in regulation of focal adhesion size and number: reciprocal regulation of caveolin-1 and β1 integrin, *Scientific reports* **7**(1), 15008. https://doi.org/10.1038/s41598-017-14932-6

Zhao, J., Cao, Y., DiPietro, L. A. and Liang, J. (2017), Dynamic cellular finite-element method for modelling large-scale cell migration and proliferation under the control of mechanical and biochemical cues: a study of re-epithelialization, *Journal of The Royal Society Interface* **14**(129), 20160959. https://doi.org/10.1098/rsif.2016.0959

Zhao, J., Naveed, H., Kachalo, S., Cao, Y., Tian, W. and Liang, J. (2013), Dynamic mechanical finite element model of biological cells for studying cellular pattern formation, *in* 2013 35th Annual International Conference of the IEEE Engineering in Medicine and Biology Society (EMBC), IEEE, pp. 4517–4520. https://doi.org/10.1109/EMBC.2013.6610551

Zielinski, R., Mihai, C., Kniss, D. and Ghadiali, S. N. (2013), Finite element analysis of traction force microscopy: Influence of cell mechanics, adhesion, and morphology, *Journal of Biomechanical Engineering* **135**(7), 071009. https://doi.org/10.1115/1.4024467